Thermochimica Acta, 180 (1991) 9–21
Elsevier Science Publishers B.V., Amsterdam

DETERMINATION OF THE KINETIC PARAMETERS OF THE REACTION BETWEEN SO_2 AND CaO USING THE THERMOGRAVIMETRIC TECHNIQUE *

A.F. SHAABAN

Department of Chemical Engineering and Pilot Plant, National Research Centre, Dokki, Cairo (Egypt)

(Received 18 July 1990)

ABSTRACT

Fibrous filters can be used to bind hazardous acidic gases (HCl, HF, SO_2, SO_3, etc.) to fine alkaline grain sorbents prior to and during their filtration. The availability of reaction kinetic data is essential for the calculation of the gas-conversion profile in a fixed-bed reactor. A thermogravimetric technique was developed for making kinetic measurements under differential boundary conditions. For the system CaO/SO_2 the weight increase with time was recorded. The present results show the possibility of verifying the use of such a technique by using minor weights of limestone powder. The experimental data obtained are well represented by the shrinkage core model. However, the coincidence between experimental values and values calculated using $CaCO_3$ pellets was unsatisfactory. The determined kinetic data can serve as a basis for the calculation of SO_2 breakthrough curves in a CaO fixed-bed reactor. The activation energy, as indicated by the slope of the Arrhenius plot, was found to be 7.5–8 kcal g^{-1} mol^{-1}. The kinetic parameters evaluated are in a good agreement with those reported in the literature.

INTRODUCTION AND PROBLEM PRESENTATION

Exhaust fumes which usually contain fine solid particles may also contain hazardous acidic gases such as HCl, HF, SO_2 or SO_3, in which case an economical process for the reduction of emissions is necessary.

The development of an alternative process that depends on the combined separation of the dust and dangerous gases in a fixed-bed reactor is quite helpful. In such a case, the alkaline solid bed (CaO, $CaCO_3$ or $Ca(OH)_2$) will simultaneously react chemically with acidic gases and will mechanically separate any particulate contaminants [16–18]. For the construction and dimensioning of such filters, with regard to the diminution of harmful gases,

* This work was done at the Institute of Mechanical Engineering, University of Karlsruhe, Germany.

0040-6031/91/$03.50

it is necessary to trace out the breakthrough curves for the SO_2/CaO reaction. However, the assessment of such curves also requires knowledge of the kinetic parameters necessary to solve the material-balance equation in a fixed-bed reactor. These kinetic data can be determined by measuring the solid conversion with time under differential boundary conditions. The latter conditions in gas/solid reactions mean that the difference in reactant gas concentration between the feed and effluent streams is not significantly affected by the reaction under study. The kinetic parameters of the reaction $CaO + SO_2 + \frac{1}{2}O_2 \rightarrow CaSO_4$ were calculated from conversion-time curves determined by means of the thermogravimetric technique through the direct recording of the weight increase during the reaction.

BALANCE ON A FIXED-BED REACTOR AND REACTION OF A SINGLE PARTICLE

The concentration of a reacting gas passing through a fixed bed of active solids is considered to be a function of the axial locus and time. The mathematical description of the process is based on the material balance of an element of volume together with the reaction of a single particle. The balance of mass gives (the nomenclature is given in Appendix 1)

$$\frac{\partial c}{\partial t} = -\frac{u_0}{\epsilon} \cdot \frac{\partial c}{\partial z} + D_z \cdot \frac{\partial^2 c}{\partial z^2} - r_v \tag{1}$$

The solution of eqn. (1) with the boundary conditions $c = c^0$ at $Z = 0$ for $t > 0$, and $U_B = a$ at $t = 0$ for $Z > 0$ gives the variation in the concentration, c, as a function of axial distance, Z, and time, t. The determination of a single particle reaction velocity and the number of particles in an element of volume, r_v, is essential for the solution of eqn. (1).

The simple unreacted-core model was selected to describe the noncatalytic reaction of CaO particles with a constant concentration of SO_2 gas. In this treatment conversion-time equations, for a first-order chemical reaction in homogeneous spherical particles, is developed:

$$r_v = \frac{3k_s(1-\epsilon)c_{A,F}(1-U_B)^{2/3}}{R_s\left(1 + \frac{k_s}{\beta}(1-U_B)^{2/3} + \frac{k_s R_K}{D_e}(1-U_B)^{1/3}\right)} \tag{2}$$

It is obvious that the kinetic parameters k_s, D_e and β can be determined by considering special cases of the shrinkage core model which has the general form

$$t = \frac{\rho_B R_s}{|\nu_B| M_B k_s c_{A,F}} \times \left[1 - (1-U_B)^{1/3} + \frac{k_s}{3\beta}U_B + \frac{k_s R_s}{6D_e}\left(3 - 3(1-U_B)^{2/3} - 2U_B\right)\right] \tag{3}$$

If the chemical reaction is the rate-controlling step with $\beta \gg k_s$ and $D_e \gg k_s R_s$, then

$$t = \frac{\rho_B R_s}{|\nu_B| M_B k_s c_{A,F}} \left[1 - (1 - U_B)^{1/3}\right] \tag{4}$$

For diffusion through ash-layer controls with $k_s R_s \gg D_e$ and $\beta \gg k_s$

$$t = \frac{\rho_B R_s^2}{6|\nu_B| M_B D_e c_{A,F}} \left[3 - 3(1 - U_B)^{2/3} - 2U_B\right] \tag{5}$$

For the mass transfer through gas-film controls with $k_s \gg \beta$ and $k_s R_s \ll D_e$

$$t = \frac{\rho_B R_s}{3|\nu_B| M_B \beta c_{A,F}} \cdot U_B \tag{6}$$

Since the kinetic parameters k_s, β and D_e are generally unknown, the experimental data may be matched against curves calculated for several values of the corresponding coefficients and the appropriate values of the coefficients are determined.

EXPERIMENTAL SET-UP AND PROCEDURE

A measurement technique using a thermobalance was developed for the experimental determination of k_s and D_e. The basic instrument used in this work was an STA 429-Netzsch-(Geratebau GMBH) which has a temperature range of 20–1600 °C, a SiC heating element, a weighing range of 0–15 g, an accuracy of ±0.02 mg and ±0.01 mg reproducibility. NiCr–Ni and PtRh 10-Pt thermocouples were used for the temperature ranges 0–1200 °C and 0–1600 °C, respectively. The temperature programming rate can be changed over 10 steps from 0.1 to 100 °C min^{-1}, and the programming mode can be changed over four steps of up, hold, down and cycle. The accuracy of temperature measurement is 0.2%. The furnace tube has a diameter and volume of 5 cm and 120 cm^3, respectively. The available measurement weighing range is 0.02–2 mg mm^{-1}. The weight and temperature were recorded on 250 mm wide punched paper. The registration unit has a six-canal compensations-point printer with 1 s frequency and a paper speed of 6–1200 mm h^{-1}. The instrument is equipped with two rotameters (0–200 cm^3 air/min) that allow thermogravimetric thermograms to be recorded in dynamic atmospheres of N_2, SO_2/N_2 and SO_2/air. The apparatus used is shown schematically in Fig. 1.

Very small weights of sample were used to guarantee differential boundary conditions. The dust-like sample was evenly distributed on an inert carrier, positioned within the reactor tube and accurately weighed. A dust generator, which disperses small amounts of powder in an air stream, was used to

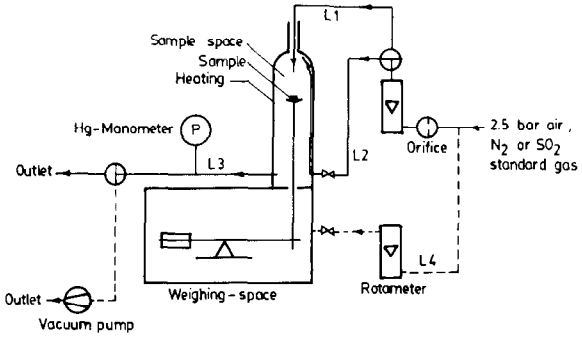

Fig. 1. Schematic representation of the experimental set-up.

accomplish the approximate individual positioning of sample particles. Limestone and calcium hydroxide powders with mean particle diameters of 10 and 6 μm, respectively, were used as sorbents. The heating rate was always set at 10 °C min^{-1}. The resulting CO_2 or H_2O vapour arising from the calcination and dehydration processes, respectively, were continuously flushed out with N_2 passing downwards (through L_1). The resulting constant-weight calcines were then sulphonated according to

$$CaO + SO_2 + \tfrac{1}{2}O_2 \rightarrow CaSO_4$$

The sample was exposed to a constant concentration of SO_2 carrier gas which was also passed downwards (or upwards through L_2).

Figure 2 shows a typical thermogram protocol of an experiment. The temperature recording during the entire measurement is presented by the dashed curve. The constant sample end temperature is approximately 650 °C. The solid curve demonstrates the weight change of the sample as a function of time. After the initial weight increase, caused by the decrease in buoyancy, a decrease in weight begins at the decomposition temperature. Figure 2 also illustrates an example of the dehydration and decomposition of a $Ca(OH)_2$

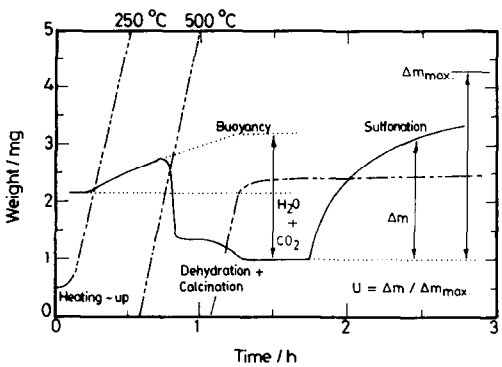

Fig. 2. Typical thermogram protocol of a sulfonation experiment.

sample containing a small amount of $CaCO_3$. The weight decrease occurs in two steps starting at 375 °C for the dehydration and 600 °C for the calcination. The weight of the CaO formed can be determined from this weight loss and the original weight of the sample. The maximum possible weight increase of the sample at the end of sulphonation, Δm_{max}, can be determined from the stoichiometry of the reaction. Thus the CaO conversion-time equation is now given by

$$U(t) = \Delta m(t)/\Delta m_{max} \tag{7}$$

In order for the experimental results to be usable in the determination of the kinetic parameters it is essential to maintain the differential boundary conditions regarding the reacting solids and to define a definite beginning of the sulphonation-reaction. Thus the concentration of SO_2 in the sample's surroundings should be increased in the form of a step input function from zero up to a nominal value. In this regard, both the sample and the weighing zones were evacuated. Before the start of the sulphonation, both zones were refilled with the reactive gas as quickly as possible without blowing off the sample. The original inlet and outlet arrangement of the flushing and reactive gases (through L_2) was used and the flow direction (through L_1) was reversed. This measurement strategy was unfortunately inefficient in maintaining the differential boundary conditions, as S-shaped conversion-time curves were obtained. This deficiency is attributed to the following effects: (1) a slow rise in SO_2 partial pressure (for 1000 ppm SO_2 inlet gas concentration, only 400–500 ppm were recorded after a long time); and (2) the increase in reaction inhibition. The former effect is probably explained by the inter- and back-mixing of gases, and short circuited gas currents at the sample position. The second effect is explained by the accumulation of the reaction product which causes the porosity to decrease and the diffusional resistance to increase (the molar volume of $CaSO_4$ is about three times larger than that of CaO). Downwards flow of both flushing and reactive gases has been shown to give more precise experimental results. The

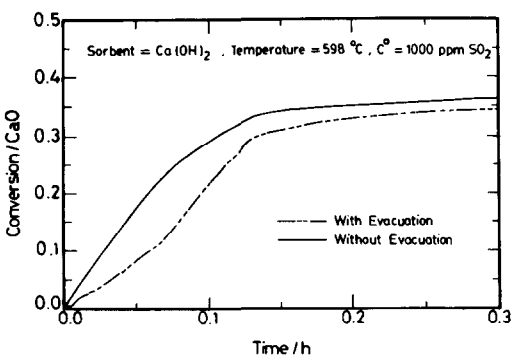

Fig. 3. Measured conversion-time data with and without evacuation of the sample space.

conversion-time data of the two experiments, for gas flowing downwards with and without evacuation before sulphonation, are shown in Fig. 3. The former method was not used further due to the impossible interpretation of the first 2 min of the reaction and the fact that S-shaped conversion-time curves were obtained. When the sample contacts the reactive gas directly the expected typical convex-shaped curve is obtained, which furnishes more accurate values of the specific reaction rate constants.

RESULTS AND DISCUSSION

The experimental results for the sulphonation of $Ca(OH)_2$ using different sample weights are shown in Fig. 4. For sample weights > 5 mg, relatively flat conversion-time curves were recorded. However, the curves became steeper as the sample weights were reduced, resulting in higher end conversion values. When very small sample weights were used the kinetic curves were of sharp convex shape as would be expected when diffusion is through ash-layer controls (eqn. (5)). Whenever the resistance of the gas film is the rate-determining step, a linear increase in conversion with time is expected (eqn. (6)). It should be noted that domination of differential boundary conditions for sample weights > 5 mg is not substantiated with the detection of an appreciable film resistance. Sample weights of 3–5 mg were used in order to guarantee that such conditions prevailed.

The dependence of reaction rate on temperature is illustrated clearly in Fig. 5. The increase in temperature results in increased velocity constants and equilibrium conversions. This behaviour is essentially attributed to higher chemical reaction rates and the acceleration of the diffusion process through the growing product layer. The experimental results measured at different SO_2 gas concentrations using $Ca(OH)_2$ powder as sorbent are shown in Fig. 6. The conversion-time curves always become steeper as the

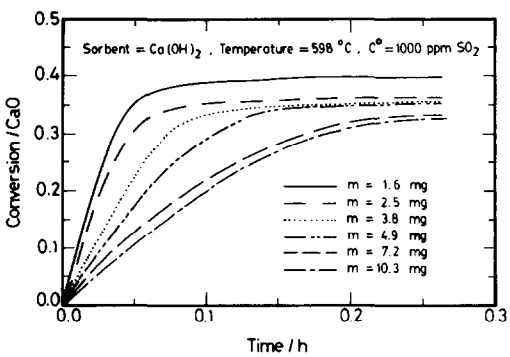

Fig. 4. Effect of sample weight on CaO sulphonation with SO_2.

TABLE 1

Kinetic data of dolomite/calcium carbonate reaction with SO_2

Ref.	E_A (kcal g^{-1} mol^{-1})	β (m s^{-1})	D_e (m^2 s^{-1})	k_s (m s^{-1})	Ref.	E_A (kcal g^{-1} mol^{-1})	β (m s^{-1})	D_e (m^2 s^{-1})	k_s (m s^{-1})
1	34.130	–	$0.4–6\times10^{-4}$	$0.65–4.75\times10^{-2}$	8	–	0.527–0.631	$7.6–14.6\times10^{-10}$	0.179–0.216
	(1029–1215 K)	–	(1029–1215 K)	(1029–1215 K)		–	$f\cdot d_p = 7.8\times10^{-4}$	(1098–1248 K)	$f\cdot d_p = 7.8\times10^{-4}$
2	13.471	–	$7.6–250\times10^{-13}$	–		–	0.30–0.358	–	0.181–0.204
	(900–1250 K)	–	(1123 K)	–		–	$f\cdot d_p = 1.55\times10^{-3}$	–	$f\cdot d_p = 1.55\times10^{-3}$
3,4	8.1–18.1	–	4×10^{-11}	$(0.22\pm0.05)10^{-2}$		–	(1098–1248 K)	–	(1098–1248 K)
	(923–1253 K)	–	(1253 K)	(1253 K)	10	–	–	$8–2500\times10^{-13}$	6.6×10^{-2}
5	37.6	–	4×10^{-11}	–		–	–	(1123 K)	(1123 K)
	(1033–1398 K)	–	(1253 K)	–	11	–	–	$6\times10^{-9}–6\times10^{-13}$	6.6×10^{-2}
6	–	–	4×10^{-11}	1.9×10^{-3}		–	–	(1123 K)	(1123 K)
	–	–	(1123 K)	(1123 K)	12	33.92	–	$0.14–1.0\times10^{-11}$	$0.3–1.16\times10^{-3}$
7	–	–	$7.5–30\times10^{-11}$	–		(1073–1223 K)	–	(1073–1223 K)	(1073–1223 K)
	–	–	(1123 K)	–		–	–	–	–
13	31 ± 3	–	–	–	21	30	–	4×10^{-11}	–
	(1073–1323 K)	–	–	–		(923–1253 K)	–	(1253 K)	–
14	11.5	–	1.8×10^{-9}	–	24	17.5	–	$4.2–7.2\times10^{-6}$	4.2×10^{-4}
	(700–1123 K)	–	(1123 K)	–		(1073–1123 K)	–	(1123 K)	(1123 K)
15	–	–	2.5×10^{-10}	6.6×10^{-2}	This	7.5–8.0	100	1.71×10^{-10}	3.1×10^{-3}
	–	–	(1123 K)	(1123 K)	work	(800–1250 K)	–	(969 K)	(969 K)
19	19.1	–	$11–63\times10^{-8}$	–		–	–	$x = 2.8\ \mu m$	$x = 2.8\ \mu m$
	–	–	(1123 K)	–		–	–	–	–

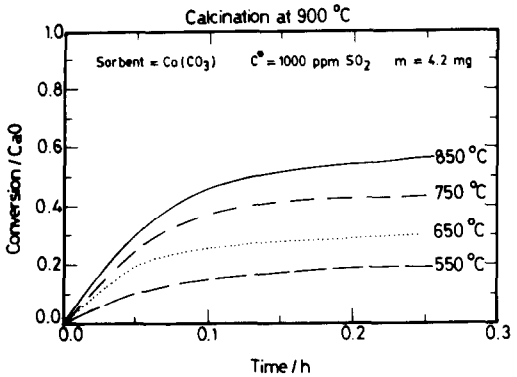

Fig. 5. Effect of temperature on CaO sulphonation with SO_2.

SO_2 concentration is increased and higher end conversions occur. The very flat curve, corresponding to $c^0 = 330$ ppm, proves the dominance of film-controlled mass transfer and the absence of differential boundary conditions. In all the experiments demonstrated in Fig. 6 the dehydration was carried out at 700 ° C using N_2 as flushing gas. The build up of both calcium sulphite and calcium sulphate in the product layer at temperatures below 500 ° C results in lower calculated CaO conversion values.

The chemical reaction considered here is only rate controlling at the very early stages of the reaction, when no product layer has been formed. In this case, the specific reaction rate constant, k_s, can be calculated using eqn. (4). Specifying the slope of the conversion-time curve at $t = 0$, one gets

$$k_s = \frac{\rho_B R_s}{3 M_B c_{A,F}} \left| \frac{\partial U}{\partial t} \right|_{t=0} \tag{8}$$

The Arrhenius plot of k_s versus $1/T$ for two experimental runs with different calcination temperatures is illustrated in Fig. 7. The activation energies corresponding to the slope of these least-squares lines are 7.5 and 8

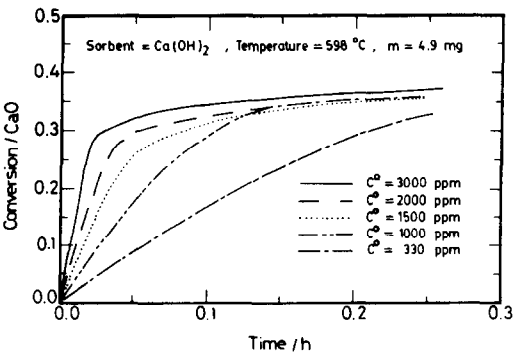

Fig. 6. Effect of SO_2 concentration on CaO sulphonation.

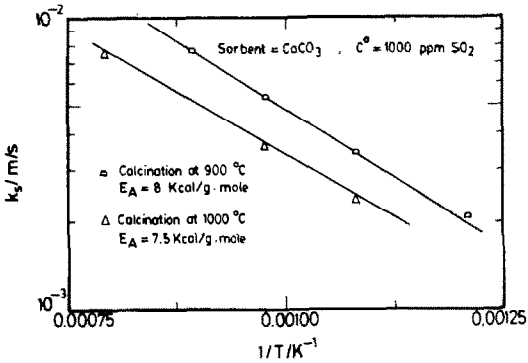

Fig. 7. Arrhenius plot for the determination of the activation energy of the $CaO + SO_2$ reaction.

kcal g^{-1} mol^{-1}. For the derivation of the core model, the reaction order was assumed to be one. Thus, based on a unit surface of unreacted core, the rate of reaction, r, is given by

$$r = \frac{1}{a \cdot \nu} \cdot \frac{dN_{SO_2}}{dt}, \quad \text{with } a = 4\pi R_K^2 \tag{9}$$

From the definition of reaction conversion and for $N_{SO_2} = N_{CaO}$

$$\frac{dU_{CaO}}{dt} = \frac{N_{CaO}^0}{a} \cdot \frac{dN_{CaO}}{dt} \tag{10}$$

Consequently,

$$r = \frac{N_{CaO}^0}{a} \cdot \frac{dU_{CaO}}{dt} = k c_{SO_2}^n \tag{11}$$

and

$$\ln \frac{dU_{CaO}}{dt} = n \ln c_{SO_2} + \ln \frac{ka}{N_{CaO}^0} \tag{12}$$

A log–log plot of dU/dt vs. SO_2 concentration for the experiments presented in Fig. 6 gives $n = 0.95$ (see Fig. 8). Neglecting the point measured

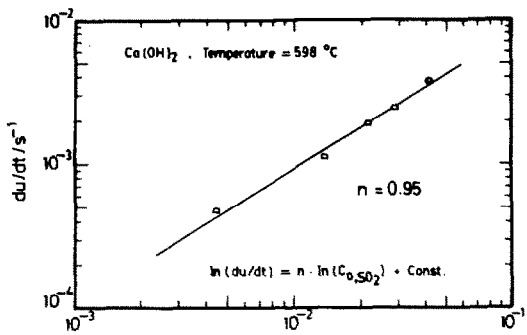

Fig. 8. Determination of the reaction order for the $CaO + SO_2$ reaction.

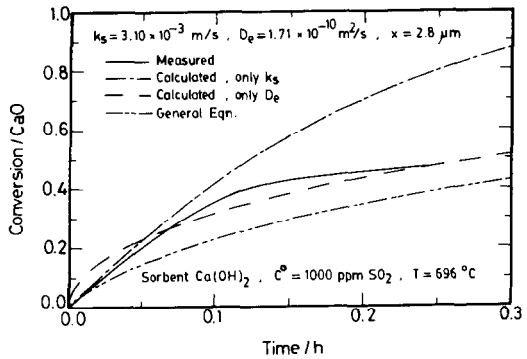

Fig. 9. Fitting of the shrinkage core model to the measured experimental data.

at 330 ppm yields $n = 1$. These results are considered as verification of the applicability of the core model.

A comparison between the experimentally determined conversion-time data and the theoretical values calculated using eqns. (3) to (5) is given in Fig. 9. The effective diffusion coefficient was determined from the experimental data by $dU/dt \rightarrow 0$. The order of magnitude of the mass-transfer coefficient, β, as evaluated using the formula of minimum sherwood's number for a single particle [22,23] was found to be 100 m s^{-1}.

It can be concluded that the experimentally determined data cannot be adequately described by using eqns. (4) and (6). Matching the data with eqns. (3) and (5) is satisfactory only in certain ranges. This is frequently due to the inhibition of the reaction by the progressive build up of product layer. Consequently, it is difficult to assign a constant value beforehand to the effective diffusion coefficient of gaseous reactant in the ash layer, D_e. The latter is believed to be a conversion-dependent parameter as expressed by the semi-empirical equation

$$D_e = D_{e0} \cdot e^{-KU} \tag{13}$$

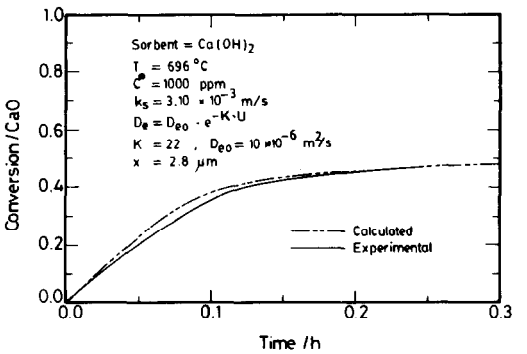

Fig. 10. Fitting of the modified core model to the measured conversion-time data.

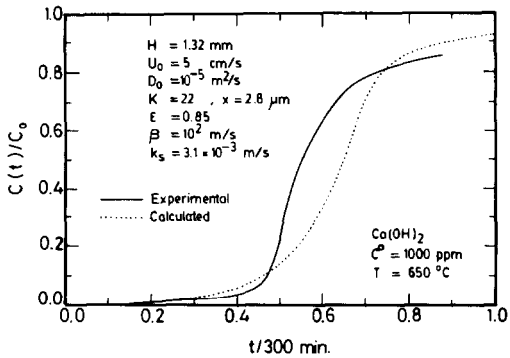

Fig. 11. Comparison between measured and calculated breakthrough curves.

Two points of the experimental U vs. t curve at extended times are generally sufficient for the calculation of D_{e0} and K. Figure 10 presents the results of this matching using the experimental data given in Fig. 9. The excellent fit of the theoretical curve and the experimental data provides a strong verification of the applicability of the theoretical model.

The kinetic data so obtained can be used to trace out the breakthrough curves for the fixed-bed filter. The results of such calculations are given in Fig. 11 where a comparison between measured (solid curve) and calculated (dotted) data is given. The calculation necessitates the numerical solution of eqn. (1) where the axial dispersion term is excluded. Moreover, the kinetic data illustrated in Fig. 10 are used as a basis for the solution of eqn. (12). The calculated curves always present a better separation than the measured ones due to random irregularities in the filter cake. The weight-average particle size of $Ca(OH)_2$ and bed porosity were 2.8 μm and 0.85, respectively. A deterioration in the separation efficiency was expected as a result of a randomly non-uniform distribution of surface-area elements and flow-channel widths in the fixed bed. It is a well known fact that there are zones of larger void fraction in the immediate vicinity of the retaining walls of the packed bed [20,22]. The measured kinetic data are in satisfactory agreement with the calculated data, despite the simplifications and assumptions used and despite the possible experimental error.

REFERENCES

1 T. Bardakci, Thermochim. Acta, 76 (1984) 287.
2 S.K. Bhatia and D.D. Perlmutter, AIChE J., 27 (1981) 226.
3 R.H. Borgwardt, Environ. Sci. Technol., 4 (1970) 59.
4 R.H. Borgwardt and R.D. Harvey, Environ. Sci. Technol., 6 (1972) 350.
5 R.H. Borgwardt and K.R. Bruce, AIChE J., 32 (1986) 239.
6 P.G. Christman and T.F. Edgar, AIChE J., 29 (1983) 388.
7 J.W. Chrostowski and C. Georgakis, Chemical Reaction Engineering, ACS Symp. Ser., No. 65, American Chemical Society, Houston, TX, 1978.

8 J.S. Dennis and A.N. Hayhurst, Chem. Eng. Sci., 41 (1986) 25.
9 E. Fitzer and W. Fritz, Technische Chemie (Technical Chemistry), Springer Verlag, Berlin, 1975.
10 C. Georgakis, C.W. Chang and J. Szekely, Chem. Eng. Sci., 34 (1979) 1072.
11 M. Hartman and R.W. Coughlin, AIChE J., 22 (1976) 490.
12 M. Hartman and O. Tranka, Chem. Eng. Sci., 35 (1980) 1189.
13 N.J. James and R. Hughes, 2nd International Conference on Control of Gaseous Sulphur and Nitrogen Compound Emissions, University of Salford, England, 1976.
14 K. Krishnaiah, R. Stein and W. Weisweiler, 21st International Seminar, University of Karlsruhe, Germany, 1986, p. 111.
15 B. Lindner and D. Simonsson, Chem. Eng. Sci., 36 (1981) 1519.
16 F. Loffler, K. Hedden, O. Balekdjian and P. Gang, Entwicklung von Verfahren zur kombinierten Abscheidung von Stauben und gasformigen Schadstoffen (Process Development for the Combined Removal of Particulate Solids and Hazardous Gases), Kernforschungszentrum Karlsruhe GmbH, KfK-PEF 26, July 1987.
17 F. Loffler and P. Gang, Kombinierte Abscheidung von Partikeln und Gasen mit Abreinigungsfiltern im Zusammenhang mit der Sorption von Gasen (Combined Removal of Particulate Solids and Gases by Fibrous Filters in Connection with the Sorption of Gases), Kernforschungszentrum Karlsruhe GmbH, KfK-PEF, March 1988.
18 F. Loffler and P. Gang, Kombinierte Abscheidung von Partikeln und Gasen mit Abreinigungsfiltern im Zusammenhang mit der Sorption von Gasen Minderung von SO_2 in Abgasen durch Reaction in Filterkuchen aus Kalzium-Verbindungen (Combined Removal of Particulate Solids and Gases by Fibrous Filters in Connection with the Decrease of SO_2 Concentration in Exhaust Fumes through its Reaction with Fibrous Calcium Compounds), Kernforschungszentrum Karlsruhe GmbH, KfK-PEF, March 1989.
19 D.W. Marsh and D.L. Ulrichson, Chem. Eng. Sci., 40 (1985) 423.
20 H. Martin, Chem. Eng. Sci., 33 (1978) 913.
21 R.L. Pigford and G. Sliger, Ind. Eng. Chem. Proc. Des. Dev., 12 (1973) 85.
22 E.U. Schlunder, Verfahrenstechnik, 10 (1976) 645.
23 E.U. Schlunder, Chem. Eng. Sci., 32 (1977) 845.
24 C.Y. Wen and M. Ishida, Environ. Sci. Technol., 7 (1973) 703.

APPENDIX 1: NOMENCLATURE

a Reaction area (m^2)
A, B, C Components A, B and C
c Concentration (kg mol m^{-3})
c^0 SO_2 initial concentration (ppm)
$c_{A,F}$ Concentration of component A in the particle surroundings (kg mol m^{-3})
d_p Particle diameter (m)
D_e Effective diffusion coefficient (m^2 s^{-1})
$D_{e,0}$ Effective diffusion coefficient for $U_B = 0$ (m^2 s^{-1})
D_z Axial dispersion coefficient (m^2 s^{-1})
E_A Activation energy (kcal g^{-1} mol^{-1})
H Bed height (mm)
k_s Specific reaction rate constant (m s^{-1})
K Constant in eqn. (13)

m	Sample weight (mg)
M_B	Molecular weight of component B (g g^{-1} mol^{-1})
n	Reaction order
N_A	Number of moles of component A (kg mol)
r_a	Reaction rate per unit area (kg mol m^{-2} s^{-1})
r_v	Effective reaction rate per unit volume of bed (kg mol m^{-3} s^{-1})
R_k	Radius of unreacted core (m)
R_s	Initial radius of solid reactant (m)
t	Time (s) (may be minutes or hours in the figures).
T	Temperature (°C)
u_0	Superficial velocity (m s^{-1})
U_B	Conversion of CaO to $CaSO_4$ (%)
x	Particle diameter (μm)
Z	Axial distance (m)
β	Mass transfer coefficient (m s^{-1})
ϵ	Bed porosity
ν_B	Stoichiometric coefficient of component B in the reaction: $\lvert\nu_A\rvert A_g + \lvert\nu_B\rvert B_s \rightarrow \lvert\nu_C\rvert C_s$
ρ_B	Density of component B (kg m^{-3})